

IMECE2017-72175

EXPERIMENTAL AND NUMERICAL STUDY OF WATER DISTILLATION PERFORMANCE OF SMALL-SCALE DIRECT CONTACT MEMBRANE DISTILLATION SYSTEM

Danielle Park
Department of Mechanical
Engineering, University of
Michigan
Ann Arbor, MI, USA

Elnaz Norouzi
Department of Mechanical and
Aerospace Engineering,
University of Missouri
Columbia, MO, USA

Chanwoo Park
Department of Mechanical and
Aerospace Engineering,
University of Missouri
Columbia, MO, USA

ABSTRACT

A small-scale Direct Contact Membrane Distillation (DCMD) system was built to investigate its water distillation performance for varying inlet temperatures and flow rates of feed and permeate streams, and salinity. A counterflow configuration between the feed and permeate streams was used to achieve an efficient heat exchange. A two-dimensional Computational Fluid Dynamics (CFD) model was developed and validated using the experimental results. The numerical results were compared with the experiments and found to be in good agreement. From this study, the most desirable conditions for distilled water production were found to be a higher feed water temperature, lower permeate temperature, higher flow rate and less salinity. The feed water temperature had a greater impact on the water production than the permeate water temperature. The numerical simulation showed that the water mass flux was maximum at the inlet of the feed stream where the feed temperature was the highest and rapidly decreased as the feed temperature decreased.

NOMENCLATURE

A area [m^2]
 C concentration
 c specific heat capacity [J/kg-K]
 D_{wv} diffusivity of water vapor [m^2/s]
 d diameter [m]
 H height [m]
 h_{fg} latent heat [J/kg]
 J mass flux [$\text{kg/m}^2\text{-s}$]
 k thermal conductivity [W/m-K]
 L length [m]
 M molecular weight [kg/mol]
 \dot{m} mass flow rate [kg/s]
 p pressure [Pa]
 q heat transfer rate [W]
 q'' heat flux [W/m^2]
 R gas constant [J/mol-K]

r radius [m]
 T temperature [K] or [$^{\circ}\text{C}$]
 U velocity in x direction [m/s]
 V velocity in y direction [m/s]
 W width [m]
 x Cartesian coordinate [m]
 y Cartesian coordinate [m]

Greek letters

δ_m thickness of membrane [m]
 ε porosity of membrane
 η thermal efficiency
 μ viscosity [N-s/m^2]
 θ angle [$^{\circ}$]
 ρ density [kg/m^3]
 τ tortuosity of membrane

Subscripts

a air
 c contact
 f feed, fluid
 fg phase change
 g gas
 i inlet
 k conduction
 kn Knudsen diffusion
 m membrane
 md molecular diffusion
 o outlet
 p permeate
 r ratio
 s solid, salt
 t thermal
 v vapor
 w water
 wv water vapor

INTRODUCTION

Membrane Distillation (MD) is a thermally-driven water distillation method used in desalination and waste water treatment. MD uses a hydrophobic, nano-porous membrane where water evaporation and/or condensation take place and water vapor flows through the membrane due to the difference in water saturation pressures of feed and permeate streams [1].

Among four variations of MD which differ according to the arrangement of each variation's permeate channel or the manner by which its channel is operated, Direct Contact Membrane Distillation (DCMD) is considered to be the simplest and most reliable configuration. This configuration consists of a hydrophobic membrane which is in direct contact with liquid phases. On one side of the membrane flows the feed water and on the other side flows the distilled water, also known as the permeate water. Because of the direct contact (small thermal resistance) of the membrane with liquids, more heat is lost through the membrane. A second variation is called Air Gap Membrane Distillation (AGMD) has the feed water in direct contact with the hot side of the membrane only. Stagnant air is introduced into a gap between the permeate side of the membrane and the condensation surface of the permeate vapor. As a result, the heat loss through the membrane is reduced, but an additional resistance of mass transfer is created, which is considered to be a disadvantage.

Vacuum Membrane Distillation (VMD) is a third MD configuration, requiring vacuum pumps to create a vacuum in the permeate membrane side. Condensation takes place outside the membrane module. Finally, in a fourth variation known as Sweeping Gas Membrane Distillation (SGMD), a non-condensable gas (air) flow sweeps the vapor from the permeate membrane side to and condenses outside the membrane module. The gas flow reduces the heat loss across the membrane and enhances the mass diffusion of water vapor. However, the main disadvantage of this configuration is that a small volume of permeate diffuses for a large sweep gas volume, requiring a large condenser because of the low partial pressures of water vapor.

When considering upgrading a membrane distillation system from an experimental scale to a larger scale, DCMD is attractive because it is the simplest configuration which implies lower costs and chances of component failure. Low operation temperatures of the feed water allow less robust power options such as renewable energy or waste heat to be viable energy sources. If waste heat is used as an energy source for DCMD, there would be no added cost because waste heat is otherwise be dissipated to the ambient. Though membrane distillation has been a topic of interest since the 1960's [2], most progress has been made in small scale applications rather than in large-scale commercial integration.

While DCMD has a lot of attractive qualities as a small-scale process, it has not been readily accepted in the industry as a commercial process. This is due to various logistic barriers such as efficient membrane material and module design, maintenance, and cost considerations. A common application for DCMD is water purification, more specifically, seawater desalination, water treatment, or removal of certain ions such as

ammonium. This is due to the typical obstacles met when trying to commercialize a new product, including mass-production membrane and module configuration, high heat loss between the feed and permeate water due to the thin membrane and its resulting lowered efficiency, and low permeate flux [1].

The membrane, made most commonly from PTFE, PVDF, or PP, is hydrophobic and has nanoscale channels so that water menisci (liquid-gas interface) are formed in their pores and exposed to the feed and permeate flows to prevent flooding (liquid flow-thru) in the nanochannels. The distribution of the pore diameter and the length of the nanochannels (tortuosity) are variables that affect the membrane distillation performance [3].

Direct Contact Membrane Distillation (DCMD) requires a temperature difference, and thus, a saturation pressure difference, between the feed and permeate channels across the membrane. This is done by running hot feed water on the evaporating side of the membrane and cooled permeate water on the condensing side. In application, the feed water would potentially be heated by renewable energy sources and waste heat from diesel engines and industrial processes [4].

Renewable and waste heat sources have been considered for MD systems showing great promise through the work of the following researchers [5-8]. Saffarini et al. performed an economic evaluation of solar-powered DCMD systems and found that a DCMD system coupled with a heat exchanger is the most cost-effective configuration, despite high conduction heat loss from the feed to the permeate water [6]. Suarez et al. performed experiments using a DCMD system driven by a Salinity Gradient Solar Pond system to measure the water production rates and associated energy consumptions [8].

Sabatly and Chiam evaluated the coupling of geothermal energy with VMD, and reported that geothermal energy could reduce the total energy consumption by approximately 95% and the cost by at least \$0.72/m³ [7]. Norouzi and Park numerically analyzed a DCMD system using the waste heat from the engine cooling system of a Diesel generator. They reported results of a parametric study varying the operating conditions of the DCMD system and changing the dimension of the MD module and heat source heat exchanger [4].

In recent years, two-dimensional CFD models have been developed by many researchers, which solve the mass, heat, and momentum transports in the flow channels of DCMD system, but the CFD models have all lacked a salt concentration equation in the feed channel [9-11]. The vertical velocity originating from the mass flux in the feed and permeate channels have also been ignored. In our CFD model, we have taken both the salt concentration equation and vertical velocity of the mass flux into account in our CFD model.

In this work, a two-dimensional CFD model was developed to study the effects of variable operating conditions such as temperature, flow rate, and salinity, on the distilled water production and thermal performance of a DCMD system. The CFD model used a permeable membrane to accurately analyze the boundary layer formation on a permeable wall. Experimental data collected from a DCMD system was used to validate the numerical results.

EXPERIMENTAL METHOD

The schematic of the DCMD experimental setup used in this study is shown in Fig. 1. The DCMD system included a feed water loop, a permeate water loop and a makeup water loop. Each loop included a DC gear pump, a fluid reservoir, a heater (for feed water loop) or a chiller (for permeate water loop), a rotameter, plumbing including a bypass for the pump and a drain, and a flow channel in the MD module. The makeup water loop consisted of a float valve and a pump that compensated for water loss from the feed loop to the permeate loop.

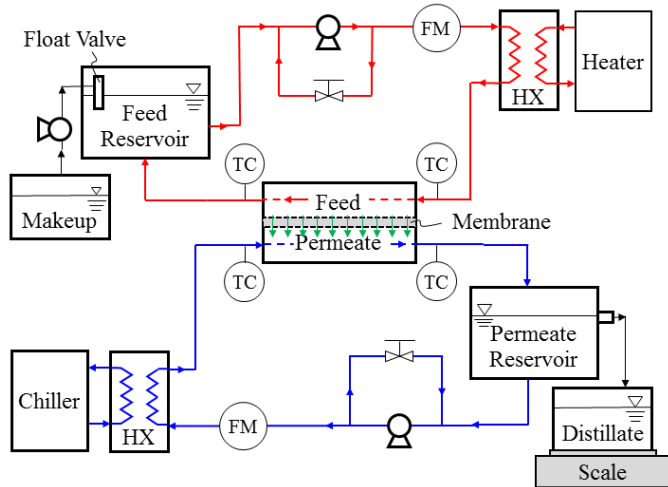


FIGURE 1. SCHEMATIC OF THE DCMD EXPERIMENTAL SETUP.

The MD module consisted of a nano-porous PTFE membrane (Clarcor, QM022) measuring 15.2 cm by 10.1 cm, sandwiched by spacers (plastic mesh), and acrylic plates on both sides. This membrane module was then clamped together by two aluminum plates for proper sealing of the flow channels using an O-ring. The aluminum plates were bolted down using bolts made of high strength grade steel.

The feed and permeate reservoirs were both constructed using CPVC piping over traditional PVC piping due to its higher temperature rating of up to 200°C. The bases of the reservoirs were also made of CPVC and the pipes and bases were glued together using CPVC cement to form the reservoir. Insulation was later added on the outer side of the feed reservoirs to reduce heat loss to ambient. PVC hose tubing was chosen for the feed and permeate flows and plastic tube fittings were chosen over brass or stainless steel due to their relatively lower cost and corrosion resistance to salt water.

In the permeate reservoir, an overflow hole was drilled into the side of the permeate reservoir. As the distillate aggregated in the permeate reservoir, the level of the water would rise and the distillate would immediately escape through the overflow hole, through which it was collected in a Pyrex flask. The flask rested on top of a scale (OHAUS, SP600) that sent continuous mass readings to the computer. Maintaining a constant water level in the feed reservoir was not only important to keep a constant salinity level in the feed water loop but also to ensure identical pressure conditions in both feed and permeate lines and the same hydrostatic pressure head in the membrane module. A level

gauge made of a clear PVC hose was added to the side of the feed reservoir to monitor the level of the water loss in the feed flow. The makeup water loop consisting of a reservoir and pump was installed for added ease in restoring the water level of the feed water reservoir as it lost water through the membrane. The float valves at the inlet of the makeup water to the feed reservoir controlled the water flow to maintain the constant feed water level.

Operation of the DC power sources (Agilent, N6701A) for the DC pumps, scale for water production measurement, and a Data Acquisition System (Keithley, 2701) used for thermocouple readings were automated using various computer software such as LabVIEW and ExceLINX. The flow rates of the feed and permeate loops were controlled by adjusting the DC voltages into the DC pumps and using the valve in a bypass line for each loop. Once steady-state conditions of the flow rates and temperatures in the permeate and feed loops were achieved, measurement of the distilled water production using a scale began.

Irregular water production was observed in the early experiments. The diagnosis of this irregularity was found to be the direct interference of the return water in the permeate reservoir exit of the distillate through overflow tube. This problem was easily resolved by attaching a tube whose one end was attached to the inlet of the permeate reservoir, and other end was submerged in the permeate reservoir water. After this remedy, the water production rates became more stable.

Steady state of each test case's conditions was defined to occur when the temperature readings remained within $\pm 0.5^\circ\text{C}$ for temperature parameters ± 2 CCM for flow rate parameters. Each set of conditions ran for 60 minutes to allow for the calculation of an average water production rate. These test cases were repeated 3 times to test for repeatability and rule out any experimental errors.

After running pure water test cases, we introduced variable concentrations of NaCl (Fisher Chemical, S271-1) in the feed flow. To measure the salinity of a sample solution, a digital refractometer (HANNA Instruments, HI96811) for brix analysis in foods was calibrated to measure the NaCl concentration of a solution. Using this calibration curve, a known volume of the feed reservoir, and a known mass of NaCl, the volume in the feed tubing was calculated. Subsequently, a corrected total volume was calculated by adding the feed tubing volume to the reservoir volume, allowing for the calculation of a more accurate dosage of NaCl needed to obtain the prescribed concentrations for our test cases.

NUMERICAL ANALYSIS

The DCMD system consists of two liquid flow channels separated by a nano-porous membrane. A Computational Fluid Dynamics (CFD) model was developed by using a commercial package, ANSYS FLUENT [12] to simulate the heat and mass transfer in the DCMD. Figure 2(a) illustrates the two-dimensional computational domain in the x - and y -directions used in the CFD analysis. The width (W_m) of the membrane channel (z - direction) was assumed to be symmetric. A

counterflow configuration between the feed and permeate streams was used to achieve an efficient heat exchange. The mass flux and conduction heat transfer across the membrane was calculated by a User-Defined Function (UDF) embedded in the FLUENT model.

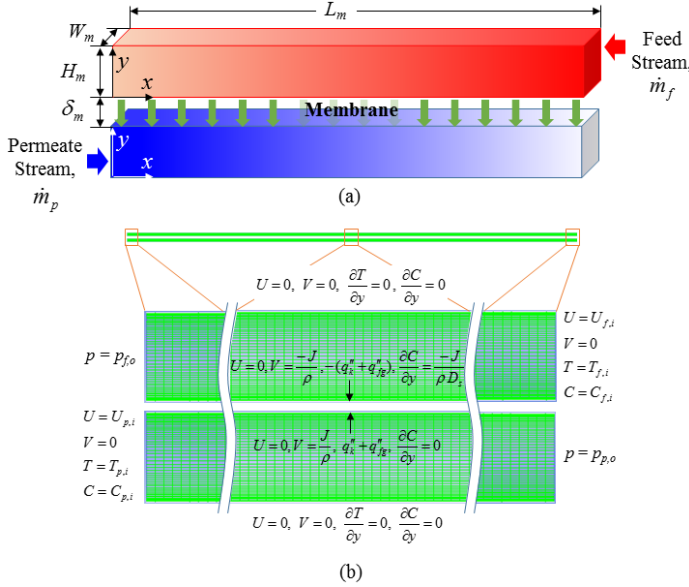


FIGURE 2. COMPUTATIONAL DOMAIN AND BOUNDARY CONDITIONS USED FOR THE CFD ANALYSIS (NOT SCALED).

The flow, heat, and mass transfer within the feed and permeate channels are governed by the conservation laws of mass, momentum, energy, and concentration. The concentration equation was solved for the feed channel only. The governing equations are given by

$$\frac{\partial(\rho U)}{\partial x} + \frac{\partial(\rho V)}{\partial y} = 0, \quad (1)$$

$$U \frac{\partial(\rho U)}{\partial x} + V \frac{\partial(\rho V)}{\partial y} = -\frac{\partial p}{\partial x} + \mu \left(\frac{\partial^2 U}{\partial x^2} + \frac{\partial^2 U}{\partial y^2} \right), \quad (2)$$

$$U \frac{\partial(\rho U)}{\partial x} + V \frac{\partial(\rho V)}{\partial y} = -\frac{\partial p}{\partial y} + \mu \left(\frac{\partial^2 V}{\partial x^2} + \frac{\partial^2 V}{\partial y^2} \right), \quad (3)$$

$$U \frac{\partial(\rho c_p T)}{\partial x} + V \frac{\partial(\rho c_p T)}{\partial y} = k \left(\frac{\partial^2 T}{\partial x^2} + \frac{\partial^2 T}{\partial y^2} \right), \quad (4)$$

$$U \frac{\partial C}{\partial x} + V \frac{\partial C}{\partial y} = D_s \left(\frac{\partial^2 C}{\partial x^2} + \frac{\partial^2 C}{\partial y^2} \right). \quad (5)$$

A velocity boundary condition was used at the inlets of the feed and permeate channels and a pressure boundary condition was used at the outlets of the channels. The boundary conditions are given by

(i) Feed or permeate channel inlets:

$$U = U_{f,i} \text{ or } U_{p,i}, \quad (6)$$

$$V = 0,$$

$$T = T_{f,i} \text{ or } T_{p,i},$$

$$C = C_{f,i} \text{ (feed water only).}$$

(ii) Feed or permeate channel outlets:

$$p = p_{f,o} \text{ or } p_{p,o}. \quad (7)$$

(iii) Impermeable walls of feed and permeate channels:

$$U = 0,$$

$$V = 0,$$

$$\frac{\partial T}{\partial y} = 0, \quad (8)$$

$$\frac{\partial C}{\partial y} = 0.$$

(iv) Feed side of permeable membrane:

$$U = 0,$$

$$V = -\frac{J}{\rho}, \quad (9)$$

$$q = -q_{fg}'' - q_k'',$$

$$\frac{\partial C}{\partial y} = -\frac{J}{\rho D_s}.$$

(v) Permeate side of permeable membrane:

$$U = 0,$$

$$V = \frac{J}{\rho}, \quad (10)$$

$$q'' = q_{fg}'' + q_k'',$$

$$\frac{\partial C}{\partial y} = 0.$$

where q'' is the heat transfer flux on the membrane including the latent heat transfer (evaporation and condensation), $q_{fg}'' (= Jh_{fg})$ and the conduction heat transfer through the membrane $q_k'' [= k_m(T_{f,m} - T_{p,m})/\delta_m]$. J is the water mass flux and δ_m is the thickness of the membrane. k_m is the effective thermal conductivity of the membrane and is given by

$$k_m = \left(\frac{\varepsilon}{k_g} + \frac{1-\varepsilon}{k_s} \right)^{-1}, \quad (11)$$

where, ε , k_s , and k_g are the porosity and the bulk thermal conductivity of the membrane material, and thermal conductivity of water vapor, respectively.

The computational domain as shown in Fig. 2(a) was meshed using structured quadrilateral cells of high skewness using a size function to assign finer meshes along the solid walls [Fig. 2(b)]. The SIMPLE algorithm was chosen for pressure-velocity coupling, and a second-order upwind discretization scheme was employed as spatial derivatives properties. The mesh quality was evaluated by checking the dependency of the results of the CFD analysis such as pressure drop of the fluid flows and water production rate on different mesh sizes. A finer mesh was used for the flow region adjacent to solid walls such as the membrane and channel walls. Considering the accuracy of the results and computation time, a mesh system consisting of 75,000 mesh elements as shown in Fig. 2(b) was chosen for the CFD analysis. The green lines in the figure represent the mesh lines which were too fine to clearly display. (For interpretation

of the references to color in this text, the reader is referred to the web version of this article.)

Round-off error is reduced by utilizing double precision for real numbers. The convergence criterion was set at 1×10^{-12} residuals for the continuity, two momentum and energy equations. In the boundary conditions, the fluid velocity normal to the wall [V in Eqs. (9) and (10)] is determined from the mass flux which is calculated in a User Defined Function (UDF) embedded in the FLUENT model. The concentration gradient at the interface of the membrane and channels can be determined from the mass flux.

The mass transfer through the nano-channel network in the porous membrane can be modeled as gas transport in porous media known as the Dusty Gas Model (DGM) and be characterized by four possible mechanisms: viscous flow, Knudsen diffusion, molecular diffusion, and surface diffusion. It is common in DCMD applications to neglect surface diffusion and viscous flow [3]. In the Knudsen diffusion mechanism, the gas density is so low or the pore size is so small that collisions between molecules can be ignored compared to collisions of molecules against the inner walls of the porous membrane. In the molecular-diffusion mechanism, molecule-molecule collisions dominate molecule-wall collisions and different species of a mixture move relative to each other under the influence of concentration gradients.

Due to the complex geometries of most membranes and a mean free molecular path of saturated water vapor under typical DCMD operating conditions comparable to the typical pore size used in MD membranes, the two mechanisms—molecular and Knudsen diffusions—may coexist in one membrane. Consequently, the transmembrane water flux can be described by a combination of the molecular and Knudsen diffusions and is given by

$$C_{kn} = \frac{2}{3} \frac{M_w}{RT_m} \frac{\varepsilon_m r_m}{\tau_m \delta_m} \sqrt{\frac{8RT_m}{\pi M_w}}, \quad (12)$$

$$C_{md} = \frac{M_w}{RT_m} \frac{\varepsilon_m}{\tau_m \delta_m} \frac{pD_{wv}}{p_a}, \quad (13)$$

$$pD_{wv} = 1.895 \times 10^{-5} T_m^{2.072}, \quad (14)$$

$$C_m = \left(\frac{1}{C_{kn}} + \frac{1}{C_{md}} \right)^{-1}, \quad (15)$$

where, pD_{wv} is a product of the total pressure (p) and water-vapor diffusivity (D_{wv}) in the unit of $[\text{Pa}\cdot\text{m}^2/\text{s}]$. ε , r_m , δ_m , and d_p are porosity, pore radius, tortuosity, thickness, and pore diameter of the membrane, respectively and their values are listed in Table 1. T_m is the membrane temperature in Kelvin and obtained by the average of the local feed and permeate temperatures ($T_{m,f}$, $T_{m,p}$) on the membrane surfaces.

The saturation pressures ($p_{v,f}$, $p_{v,p}$) of the feed and permeate water streams are evaluated at the respective local fluid temperatures on the membrane surfaces (Antoine equation) is given by

$$p_v = \exp \left(23.1964 - \frac{3816.44}{T_f - 46.13} \right), \quad (16)$$

where, the fluid temperature, T_f is in the unit of Kelvin. The fluid saturation pressure, p_v is in the unit of Pascals. The saturation pressure of a binary fluid is calculated by Raoult's law [1] and is given by

$$p_v = (1 - C)p_s, \quad (17)$$

where, p_v , p_s , and C are the vapor pressure in the unit of Pascals, the saturation pressure in the unit of Pascals and the concentration of a binary solution, respectively.

TABLE 1. DIMENSIONAL AND THERMOPHYSICAL PROPERTIES OF THE MEMBRANE USED IN THE DCMD SYSTEM.

Dimensional and thermophysical properties of membrane						
Membrane type	δ_m (m)	d_m (m)	ε	τ	k_m (W/m-K)	θ_c ($^\circ$)
QM022	84×10^{-6}	3.6×10^{-7}	0.62	2.34	0.23	127

The mass flux across the membrane is given by

$$J = C_m (p_{v,f} - p_{v,p}), \quad (18)$$

and the water production rate is given by

$$\dot{m}_w = JA_m, \quad (19)$$

where, the membrane area, $A_m = W_m L_m$.

The thermal efficiency of the DCMD system can be defined by the ratio of the phase change heat transfer to the total heat transfer across the membrane which is used to measure the efficiency of the thermal energy utilization for the membrane distillation, and is given by

$$\eta_T = \frac{q_{fg}}{q_{fg} + q_k}, \quad (20)$$

where,

$$q_{fg} = W_m \int_0^{L_m} q_{fg}'' dx, \quad (21)$$

$$q_k = W_m \int_0^{L_m} q_k'' dx. \quad (22)$$

RESULTS AND DISCUSSION

We investigated the characteristics of the distilled water production to varying inlet feed temperatures against the baseline inlet permeate temperature, and varying inlet permeate temperatures against the baseline inlet feed temperature. The ranges of the variables used in this study are listed in Table 2.

TABLE 2. OPERATING CONDITIONS AND DIMENSIONS OF THE DCMD SYSTEM.

Operating conditions (baseline conditions)			
$T_{f,i}$ ($^\circ\text{C}$)	$T_{p,i}$ ($^\circ\text{C}$)	$\dot{m}_f = \dot{m}_p$ (g s^{-1})	C (mol/L)
45 ~ 75 (60)	10 ~ 40 (25)	4.8 ~ 14.5 (9.7)	0.129 ~ 0.746 (0)
Dimensions of the DCMD system			
L_m (mm)	H_m (mm)	W_m (mm)	
152	1	101	

The baseline conditions for variables are included in parentheses. The baseline inlet feed and permeate temperatures were 60 and 25°C, respectively. For simplicity, the feed and permeate flow rates were set to be equal ($\dot{m}_f = \dot{m}_p$). The baseline flow rate of feed and permeate streams was 9.7 g/s (or 581 CCM). The inlet feed temperature varied from 45°C to 75°C in increments of 5°C, while the inlet permeate temperature varied from 10°C to 40°C in increments of 5°C as listed in Table 2.

Figure 3(a-b) shows the numerical results of the variations of the feed and permeate temperatures along the flow directions. Note that x -direction is aligned with the feed flow direction but is opposite to the permeate flow direction (i.e., counterflow configuration). It is observed in Fig. 3(a) that the rapid changes in the temperatures at the inlets are due to the developing flows in the flow channels. The conduction heat transfer (q_k'') across the membrane remains constant due to the relatively constant temperature difference across the membrane. In contrast, the latent heat transfer (q_{fg}'') rapidly decreases as the feed water temperature decreases and thus, the saturation pressure difference decreases.

Figure 3(c) shows the variations of the saturation pressure difference (Δp_v) between the feed and permeate streams which rapidly decreases because of the steep change in the saturation pressure of water, especially in the feed stream at higher temperatures, according to the Antoine relation in Eq. (16). Since the water mass flux (J) is mainly determined by the pressure difference across the membrane, it shows the changes are similar to that of the pressure difference.

Figure 4 shows that as the feed temperature increased, the water production rate also increased linearly. In Fig. 5, increasing the inlet permeate temperature caused water production to decrease because the temperature difference between the feed and permeate streams, and in effect, the pressure difference across the membrane decreased. This confirms that the water production is greatly determined by the difference of the saturation pressures of the feed and permeate water at the temperatures on each side of the membrane. Interestingly, the feed temperature affects the mass flux much more than the permeate temperature. This is because of the large variation of the water saturation pressure at higher temperatures [Antoine relation Eq. (16)]. The comparison between the experimental data and CFD models shows that there is a 7% error for the water production in cases of variable feed and permeate temperatures. This error could emerge from instrument error and simplifications existing in the CFD model such as negligible heat loss.

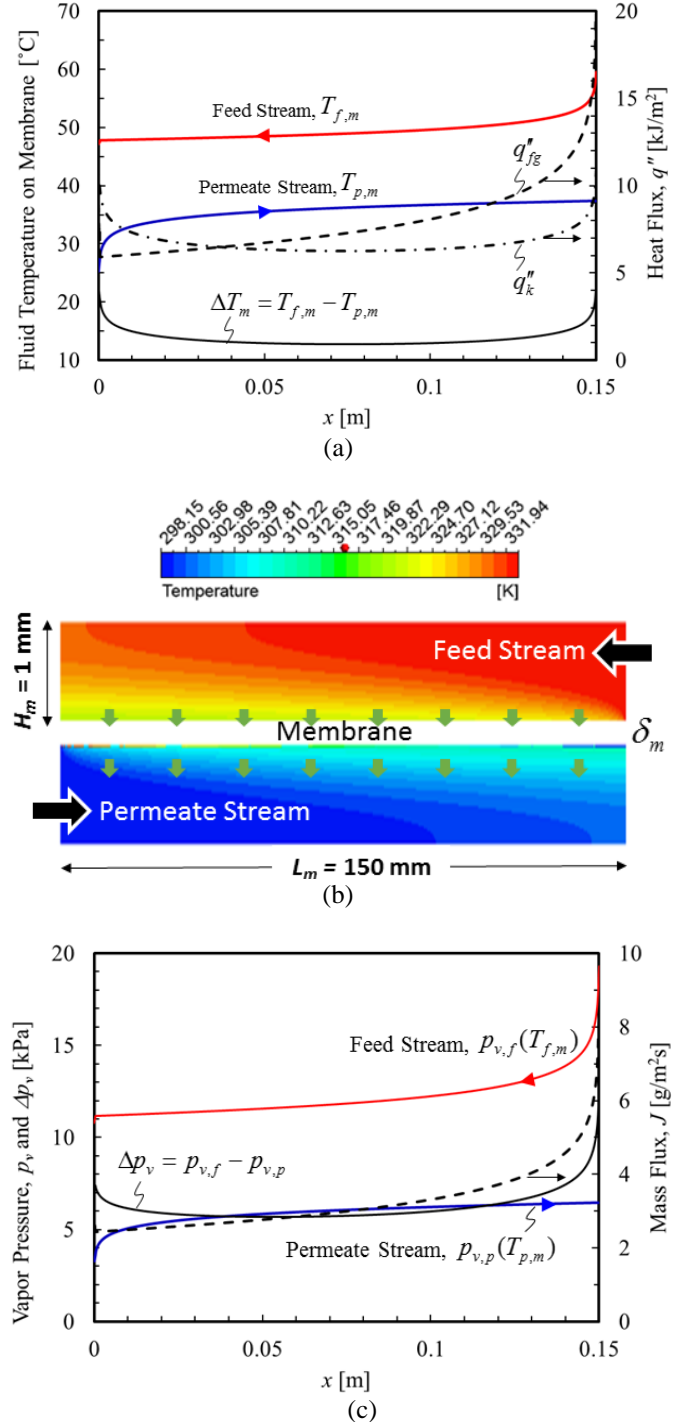


FIGURE 3. (a) VARIATIONS OF THE TEMPERATURES OF THE FEED AND PERMEATE STREAMS AND HEAT TRANSFER RATES ON THE MEMBRANE. (b) TEMPERATURE CONTOURS IN THE FEED AND PERMEATE CHANNELS (NOT SCALED). (c) VARIATIONS OF THE SATURATION PRESSURES OF THE FEED AND PERMEATE STREAMS ON THE MEMBRANE AND WATER MASS FLUX OF THE DCMD SYSTEM.

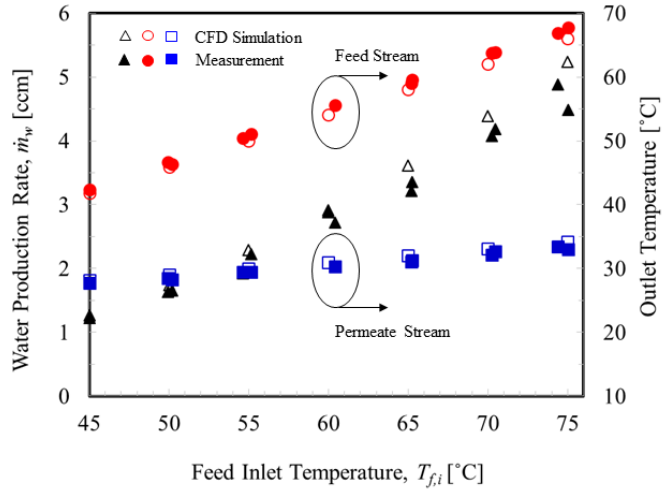


FIGURE 4. EFFECT OF FEED TEMPERATURE ON DISTILLATE WATER PRODUCTION.

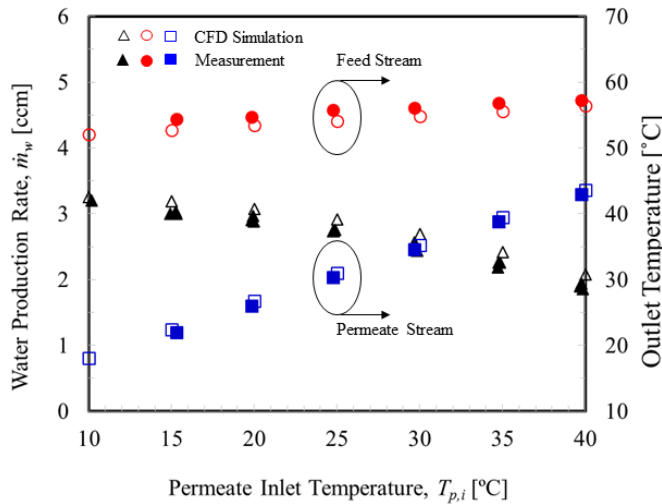


FIGURE 5. EFFECT OF PERMEATE TEMPERATURE ON DISTILLATE WATER PRODUCTION.

The effects of adjusting the flow rates of the feed and permeate water on the distilled water production was also investigated and the results are shown in Fig. 6. We chose our baseline flowrate to correspond to an inlet velocity of 10 cm/s ($U_{f,i} = U_{p,i}$) and defined our lower bound inlet velocity to be 5 cm/s and our upper bound inlet velocity to be 15 cm/s. The flow rates for the feed and permeate loops are equal in this study. Using these inlet velocities, the feed and permeate flow rates were calculated providing flow rates ranging from 290 CCM (4.8 g/s at room temperature) to 872 CCM (14.5 g/s). As the flow rates were increased, water production also increased due to a higher mass transfer rate and therefore uniform temperatures are achieved along the MD channels. The maximum error for water production is 22% with overestimation of the water production for the lower bound flow rate (290 CCM). The cause might be the heat loss in the experiment which is not considered in CFD model.

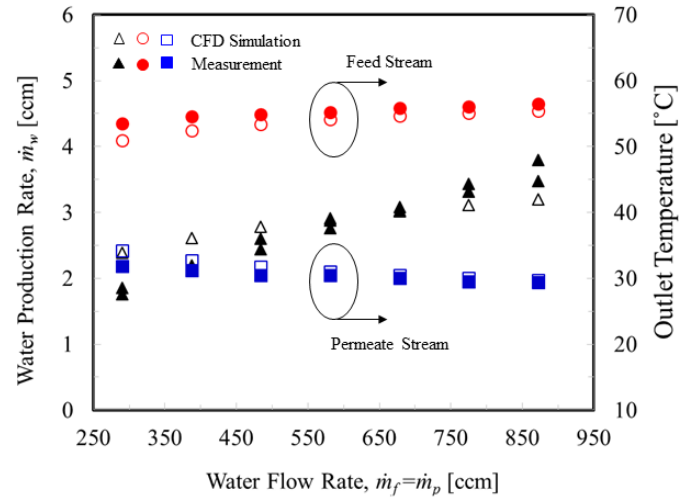


FIGURE 6. EFFECT OF MASS FLOW RATES OF THE FEED AND PERMEATE STREAMS ON DISTILLATE WATER PRODUCTION.

Since a possible application for the DCMD is desalination of ocean water whose concentration averages around 35 g/L (0.599 M), the salinity of ocean water was captured in the concentration range for the salt water experiments (NaCl/water mixture). The NaCl concentration was set to range from 0 to 0.7 M. It was observed in Fig. 7(a) that when the concentration of NaCl in the feed water increased, the water production rate decreased. This is because the presence of NaCl molecules impedes the phase change and thus reduces the water vapor transport through the membrane. As a result, the concentration of salt in the feed water decreases the saturation pressure as according to Raoult's Law [Eq. (17)].

The variation of the salt concentration in the membrane on the feed channel's side and its associated saturation pressure for the highest salt concentration (0.7 M) is shown in Fig. 7(b). The effect of the salt concentration on the saturation pressure is negligible. Therefore, the change of the saturation pressure is mainly due to the temperature variation of the feed stream.

Figure 7(c) shows the concentration contour in the feed channel and the concentration boundary layer (polarization) near the membrane where the concentration greatly varies over a thin layer on the membrane due to water distillation. The largest error between experimental data and CFD simulation results of the water production occurs for the upper bound salinity solution (0.7 M), at 29%. Raoult's model formulates vapour pressure for an ideal solution. Since no solution is completely ideal, the error increases with the increase of positive and negative charges in the solution.

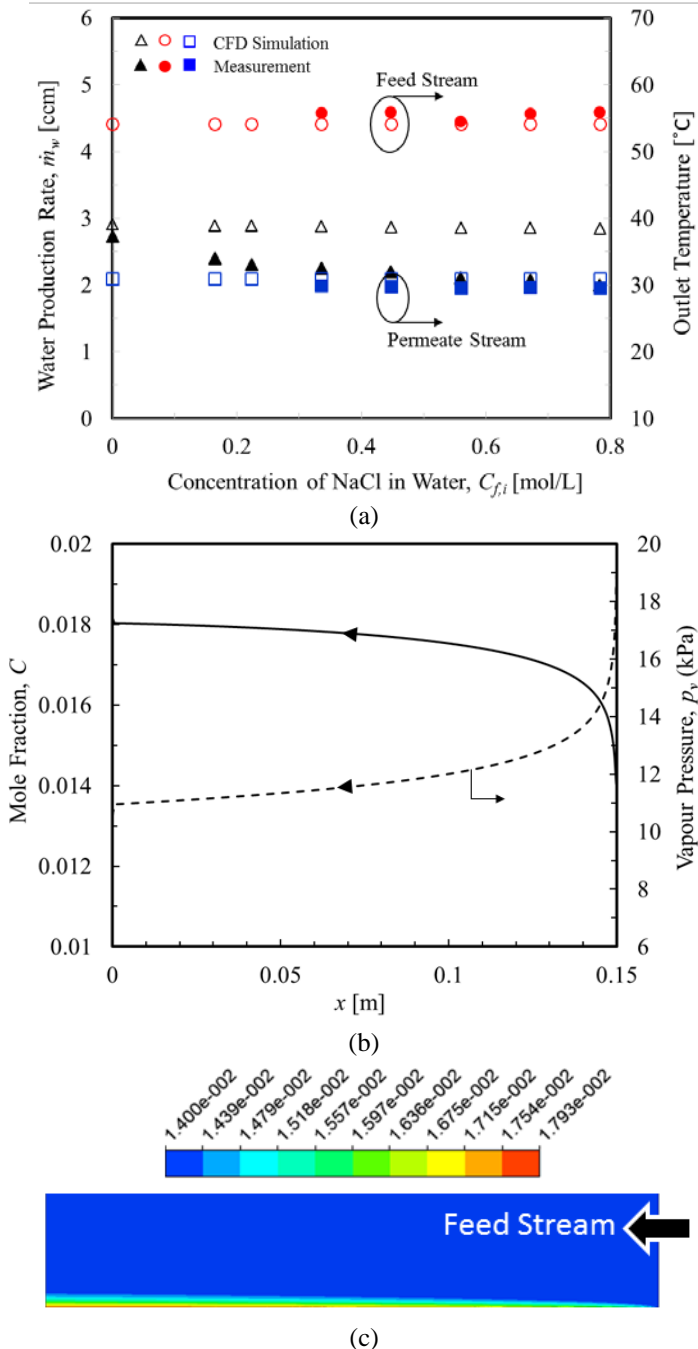


FIGURE 7. (a) EFFECT OF NaCl CONCENTRATION IN THE FEED STREAM ON DISTILLATE WATER PRODUCTION. (b) VARIATION OF NaCl CONCENTRATION ON THE MEMBRANE and (c) CONTOUR OF THE NaCl CONCENTRATION IN THE FEED CHANNEL OF THE DCMD SYSTEM (NOT SCALED).

CONCLUSIONS

The water distillation performance of a small Direct Contact Membrane Distillation (DCMD) system was studied using an experimental measurement and numerical simulation. The main operating conditions such as temperatures, flow rate of the feed

and permeate streams, and salinity were manipulated to study their effect on the water distillation performance. In the numerical simulation, a two-dimensional CFD model used to analyze the conjugate heat and mass transports in the DCMD system and validated by experimental results. The comparison between the experimental and simulation results shows good agreement. It was found that a higher feed water temperature, lower permeate temperature, higher flow rate, and less salinity produce more distilled water, and the feed temperature had more impact on the water production than the permeate temperature.

ACKNOWLEDGEMENTS

The authors extend their thanks for the financial support of the U.S. Department of Defense (DOD) and Strategic Environmental Research and Development Program (SERDP) (Contract No. W912HQ-14-C-0051), U.S. Environmental Protection Agency (EPA) (Contract No. 83533302) and National Science Foundation (IIA-1301726 and CAREER Award 1464504). The authors would also like to thank CLARCOR Industrial Air for providing the membrane samples used in the experiment. The authors alone are responsible for any omissions or other errors.

REFERENCES

1. Alkudhiri, A., N. Darwish, and N. Hilal, *Membrane distillation: A comprehensive review*. Desalination, 2012. **287**: p. 2-18.
2. Tomaszewska, M., *Membrane Distillation - Examples of Applications in Technology and Environmental Protection*. Polish Journal of Environmental Studies, 2000. **9**(1): p. 27-36.
3. Phattaranawik, J., R. Jiratananon, and A. Fane, *Effect of pore size distribution and air flux on mass transport in direct contact membrane distillation*. Journal of membrane Science, 2003. **215**(1): p. 75-85.
4. Elnaz Norouzi, C.P., *Numerical Analysis of Energy and Mass Flow of Waste Heat-Driven Direct Contact Membrane Distillation System*. Desalination, 2017: p. Under review.
5. Banat, F. and N. Jwaied, *Economic evaluation of desalination by small-scale autonomous solar-powered membrane distillation units*. Desalination, 2008. **220**(1): p. 566-573.
6. Saffarini, R.B., E.K. Summers, and H.A. Ararat, *Economic evaluation of stand-alone solar powered membrane distillation systems*. Desalination, 2012. **299**: p. 55-62.
7. Sarbatly, R. and C.-K. Chiam, *Evaluation of geothermal energy in desalination by vacuum membrane distillation*. Applied Energy, 2013. **112**: p. 737-746.
8. Suárez, F., S.W. Tyler, and A.E. Childress, *A theoretical study of a direct contact membrane distillation system coupled to a salt-gradient solar pond for terminal lakes*

- reclamation*. water research, 2010. **44**(15): p. 4601-4615.
9. Ghadiri, M., S. Fakhri, and S. Shirazian, *Modeling and CFD simulation of water desalination using nanoporous membrane contactors*. Industrial & Engineering Chemistry Research, 2013. **52**(9): p. 3490-3498.
 10. Hasanizadeh, M., et al., *CFD simulation of heat and mass transport for water transfer through hydrophilic membrane in direct-contact membrane distillation process*. Desalination and Water Treatment, 2016. **57**(39): p. 18109-18119.
 11. Janajreh, I., D. Suwwan, and R. Hashaiekeh, *Assessment of direct contact membrane distillation under different configurations, velocities and membrane properties*. Applied Energy, 2017. **185, Part 2**: p. 2058-2073.
 12. ANSYS®, *Academic Research, Release 18.0*.